Frequency Dependent Squeezed Light in Optomechanical Systems

Matthew Winchester[1]
Mentors: Sheon Chua[2], Pierre-Francois Cohadon[2]

[1]University of Colorado, 440 UCB, Boulder, CO 80309, USA
[2]Laboratoire Kastler-Brossel, Sorbonne Universités UPMC, ENS, CNRS, Collège de France, Campus Jussieu, Paris, France

Abstract. The sensitivity of gravitational wave interferometers, such as LIGO and Virgo, is currently limited by quantum noise at mid and high frequency detection bands. Further reducing quantum noise across the entire detector bandwidth will require the injection of frequency dependent squeezed light. A bright frequency dependent squeezed light source is being constructed at the Laboratoire Kastler-Brossel that will be used to interrogate an optomechanical resonator with the goal of pushing the measurement sensitivity below the standard quantum limit. This project focuses on the assembly and characterization of several components that will be used in the experiment. Results from this work will be useful for informing the future design of squeezed vacuum sources for gravitational wave interferometers.

Table of Contents

1   Introduction

1.1   Gravitational Wave Detectors and Quantum Noise

The recent detections of gravitational waves [LSC (2016)] caused by coalescing black holes have confirmed the theoretical prediction made by Einstein one hundred years ago. As the relatively young field of gravitational wave astronomy continues to mature, a never-ending battle is being fought by scientists and engineers to increase the sensitivity of gravitational wave interferometers. Further improving the sensitivity of these interferometers will increase detector range and allow the detection of weaker signals from a variety of astrophysical sources. A plot of the designed Advanced LIGO noise floor is shown in Figure 1.
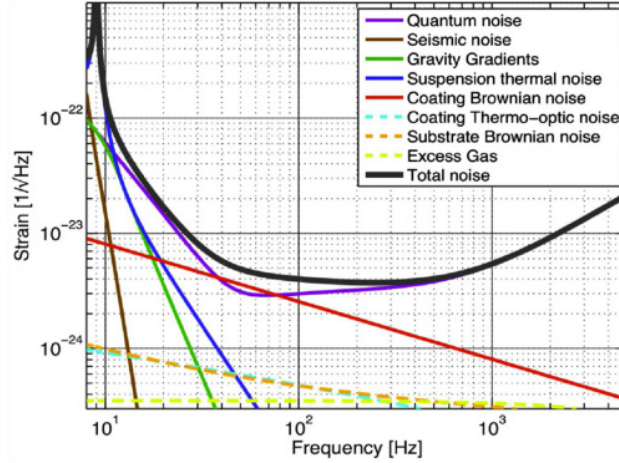

Fig. 1: Advanced LIGO noise floor. Image credit: [GWINC v3]

Quantum noise is currently limiting the precision of gravitational wave detectors in the mid and high frequency detection bands. This noise comes from two different effects. Radiation pressure noise is the result of random amplitude fluctuations on the interferometer laser. These amplitude fluctuations drive the movable test masses and get converted into phase fluctuations which can mask signals caused by gravitational waves. This noise get worse as laser power increases since the size of these amplitude fluctuations also increases. The quadrupole suspensions that hold the test masses act as low pass filters, resulting in a rapid attenuation of radiation pressure noise with frequency. The other contribution to quantum noise is shot noise, which is an uncertainty in the phase of the electromagnetic field due to the discrete nature of photons. Shot noise is reduced by increasing laser power and is frequency independent. The combination of these two processes results in the total quantum noise curve shown earlier. The point where radiation pressure noise and shot noise are equal is known as the standard quantum limit, which is around 60Hz in Advanced LIGO.

Caves (1981) originally proposed that quantum noise could be reduced by appropriately modifying the noise properties of the vacuum at the dark port of the interferometer by using squeezed states of light.

1.2 Squeezed Light

The Hamiltonian of an electromagnetic field is given by

$$\hat{\mathcal{H}} = \sum_k \hbar\omega_k(\hat{a}_k^\dagger \hat{a}_k + \frac{1}{2})\,, \tag{1}$$

where $\hbar$ is the reduced Planck constant, ω_k is the mode's angular frequency, and $\hat{a}_k^\dagger, \hat{a}_k$ are the boson creation and lowering operators respectively [Chua et al. (2014)]. The amplitude quadrature $\hat{X}_1$ and phase quadrature $\hat{X}_2$ can then be defined as

$$\hat{X}_1 = \hat{a} + \hat{a}^\dagger \tag{2}$$
$$\hat{X}_2 = i(\hat{a} - \hat{a}^\dagger) \tag{3}$$

These operators correspond to incompatible observables. The Heisenberg uncertainty between these two observables is

$$\Delta X_1 \Delta X_2 \geq 1\,, \tag{4}$$

which is analogous to the familiar position/momentum uncertainty relation. This relationship indicates that the uncertainty in one quadrature can be reduced at the expense of the other, which is known as a squeezing. It is convenient to represent the amplitude and phase quadratures of a light field using "ball-and-stick" diagrams, several of which are shown in Figure 2.

(a) Coherent State   **(b)** Vacuum State   **(c)** Amplitude Squeezed Vacuum State
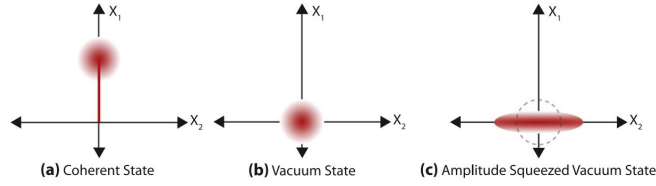
Fig. 2: Several quantum light states. (a) is a coherent state, satisfying the lower bound of equation 4 with both quadrature uncertainties equal. (b) is a coherent state with a mean amplitude of zero, i.e. a vacuum state. (c) is an amplitude squeezed vacuum state. Image credit: [Chua et al. (2014)]

Squeezed light states are of interest to the gravitational wave community because they offer the ability to reduce the quantum noise limits of detectors. For example, radiation pressure noise at low frequencies can be lowered by squeezing the amplitude quadrature. However this also results in a larger uncertainty (anti-squeezing) in the phase amplitude, which actually increases shot noise. The reverse case is also true: phase quadrature squeezed light improves shot noise performance at high frequencies but increases radiation pressure noise. These examples are meant to illustrate that in order for squeezed light to be beneficial at all frequencies, squeezing needs to be frequency dependent. Figure 3 shows how the quantum noise curve depicted earlier can be modified by injecting a vacuum state squeezed along different quadratures, as well as the quantum noise when the squeezing is optimally applied for all frequencies.

Frequency dependent squeezed light can be created by injecting frequency independent squeezing (usually generated with nonlinear crystals, atoms, or optomechanics) into
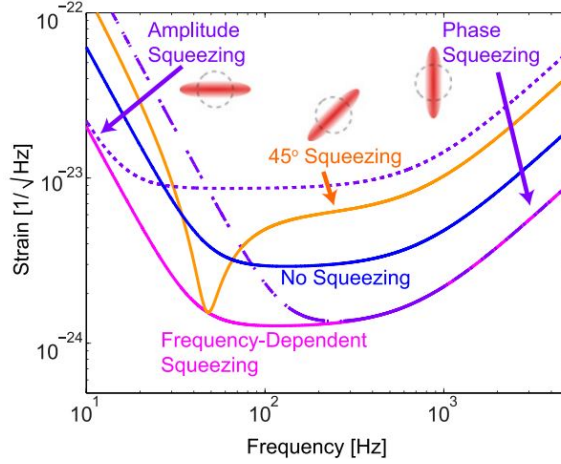
Fig. 3: Effects of frequency dependent and independent squeezing on the quantum noise curve shown previously. Optimal noise reduction across the entire detection band requires frequency dependent squeezing. Image credit: [Chua et al. (2014)]

a rotation cavity. A Fabry-Perot cavity detuned from the squeezed carrier frequency is one example of a rotation cavity. Far from cavity resonance, sideband don't interact with the cavity so the sideband pairs are in amplitude modulation (phase squeezing). The phase-dispersion of the cavity causes sidebands near cavity resonance to be phase shifted by 180 degrees resulting in phase modulation (amplitude squeezing). This process is depicted in Figure 4.

The frequency bandwidth required to go from pure amplitude squeezing to pure phase squeezing is roughly the linewidth of the rotation cavity resonance. For gravitational wave interferometers, this is on the order of 100Hz. Creating an optical cavity with such a narrow linewidth is a technically demanding task and remains an active area of development. However, the optomechanical experiment described in the following section will use frequency dependent squeezed light to probe a mechanical oscillator in a much higher frequency domain, requiring a rotation cavity with a linewidth on the order of 100kHz, thus having less stringent constraints.

1.3   The ExSqueez-HF Experiment

The Optomechanics and Quantum Measurements group at the Laboratoire Kastler Brossel (LKB) is currently building a squeezing experiment known as ExSqueez High Frequency (ExSqueez-HF) which will be used to test frequency dependent squeezing with a cryogenically cooled optomechanical resonator described in [Kuhn et al. (2014)]. A simplified optical setup for the squeezed light source is shown in Figure 5.

This project focused on four key components of the experiment. The infrared mode cleaner cavity (MC-IR) was optically characterized and locked the the main laser. The rotation cavity (RC) was assembled, followed by similar optical characterization and locking tests. The optical parametric oscillator (OPO) was assembled, and the nonlinear gain curve was measured. Lastly, the second harmonic generator (SHG) was assembled and successfully locked to the main laser. The rest of this report describes this work in detail and concludes with a brief overview of the remaining work necessary to generate a frequency dependent squeezed light source.
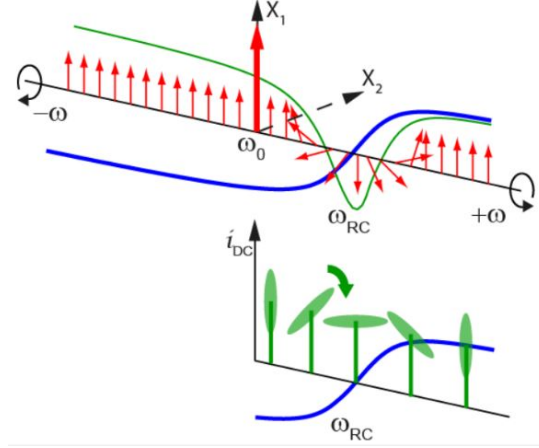
Fig. 4: Carrier-sideband picture of frequency dependent squeezing. The rotation cavity phase-dispersion (blue trace) causes sidebands near resonance ω_{RC} to be phase shifted 180 degrees. The lower plot shows the squeezing ellipse rotating from phase squeezing to amplitude squeezing to phase squeezing again as the cavity resonance is crossed. Image credit: [Chua et al. (2014)]
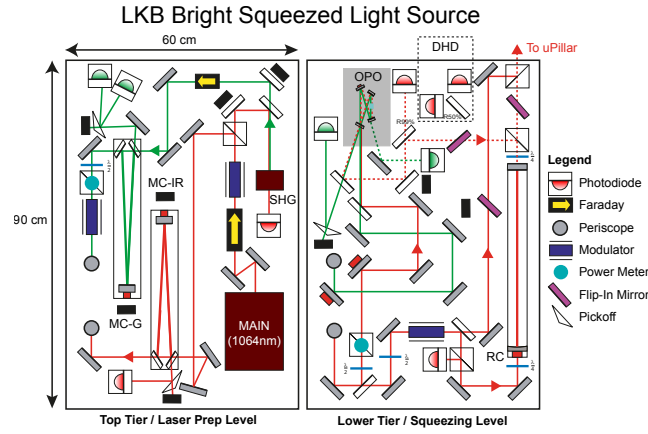

Fig. 5: Optical layout of the full ExSqueez experiment. The project details work done on the MC-IR, RC, OPO, and SHG stages.

2   Python Red Pitaya Lockbox (PyRPL)

PyRPL is a software package used for implementing feedback loops and diagnostics on Red Pitaya FPGA boards; one board is shown in Figure 6. It was created by the Optomechanics and Quantum Measurements group at LKB and is still in active development. PyRPL creates feedback control loops by utilizing different modules such as PID controllers, IIR filters, and IQ quadrature modulation/demodulation. PyRPL also allows the FPGA to function as many different laboratory instruments simultaneously, such as an oscilloscope, arbitrary signal generator, spectrum analyzer, and network analyzer. A major component of this project was using PyRPL to lock several optical cavities to a reference laser using different control schemes. The vast majority of data in this report was also digitally acquired using PyRPL.
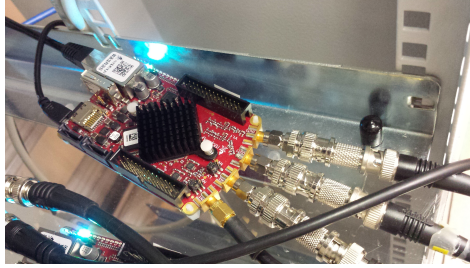

Fig. 6: A Red Pitaya FPGA board with several inputs and outputs connected to BNC cables.

2.1   Qualitative Locking Algorithm Description

All locking techniques are implemented in PyRPL using essentially the same steps. Creating a lock requires two inputs to the FPGA: the error signal and either a transmission or reflection signal from a photodetector which is used to determine whether or not the cavity is on resonance. Once the appropriate input signals have been sent to the FPGA, the cavity PZT is swept by the FPGA over its full output range of $\pm 1V$ which is then increased to $\pm 50V$ by an external high voltage amplifier. This is a sufficient range to clear at least 1 free spectral range (FSR) on all cavities to be used in the squeezing experiment. The FPGA then performs a smaller calibration sweep which is triggered upon reaching a transmission maximum or reflection minimum which indicates a cavity resonance. These maxima/minima are stored by PyRPL and used to determine whether or not the cavity is resonant.

To lock the cavity, PyRPL then turns on feedback by sending the error signal to a PID module on the FPGA. The PID module attempts to bring the error signal to zero (or a desired set point) by driving an actuator, (normally a PZT on a cavity mirror), hence locking the cavity to the reference laser.

The physical parameters of the system, such as cavity length, cavity finesse, and piezomechanical response that are needed for the calibration stage are stored in a 'config' YML file which is then used by PyRPL. PyRPL also fits theoretically modeled curves to reflection/transmission and error signals which are used to calculate the slope of these signals at the set point. This information is needed for correctly scaling the gain settings of the PID controller. The config file also contains a list of the inputs and outputs that

will be used for the lock. Storing this information in a config file offers the advantage of making the rest of the PyRPL code very generic; implementing a locking technique on any given cavity simply requires creating or modifying the config file.

Another advantage of PyRPL is that multi-stage locks can be easily implemented. A typical locking scheme will start by sweeping PZT until a certain transmission/reflection threshold is measured, engaging an intermediate side-of-fringe lock using this signal, then finally engaging a more stable lock like PDH on the cavity resonance. Schemes like this are useful because they don't require manually scanning the PZT around until the appropriate region of an error signal is found.

Specific examples of the cavity locks set up using PyRPL are more thoroughly discussed in the following sections.

3   Mode Cleaner Cavities

Mode cleaner cavities are optical resonators used to filter the spatial and spectral profiles of an incident laser beam. When a cavity is locked to a laser (or vice versa), all higher-order modes of the laser are strongly attenuated by the cavity so that only the resonant TEM_{00} mode is transmitted.

The complete squeezing experiment will employ two triangular cavities as mode cleaners. These mode cleaners will attenuate laser frequency noise, ideally bringing the lasers to shot noise limited performance at the desired Fourier frequencies of interest. Mode cleaners are needed for for both the main laser at 1064nm and the second harmonic beam at 532nm.

3.1   Optical Characterization

Before being used in the squeezing experiment, the mode cleaners must be properly aligned so that as much power is coupled into the TEM_{00} mode as possible. Several important optical properties must also be characterized to confirm that the cavities will adequately filter incident light.

The free spectral range (FSR) of an optical cavity is defined as:

$$\Delta\nu_{FSR} = \frac{c}{L}\,, \tag{5}$$

where c is the speed of light and L is the round-trip optical path length of the resonator. The FSR is the frequency spacing between successive resonant modes of the cavity. Both mode cleaners have an optical path length of 84cm, so $\Delta\nu_{FSR} = 357$MHz. This can be verified by sweeping the frequency of a probe laser or equivalently by sweeping the length of the cavity, and measuring the transmitted light on a photodetector. Figure 7 shows a single FSR of the mode cleaner cavity in the time domain. This signal was generated by driving a piezoelectric transducer (PZT) attached to one of the cavity mirrors in order to modulate the cavity length.

The large transmission features at times $t = 0$ms and $t = 18$ms are two successive TEM_{00} modes. The smaller transmission peaks correspond to residual power in higher order modes. 20MHz sidebands generated with an electro-optic modulator (EOM) are also present around each TEM_{00} peak and serve as a frequency scale reference. FSR traces like are useful for tuning cavity alignment in real time to couple as much light into the TEM_{00} mode as possible while reducing the power in higher order modes.

The full width at half maximum (FWHM) of the cavity resonance is also important, as this parameter determines how selective the cavity will function as a filter. The linewidth of a resonance, denoted in angular frequency units as κ, is measured using the same method described above for recording a FSR.
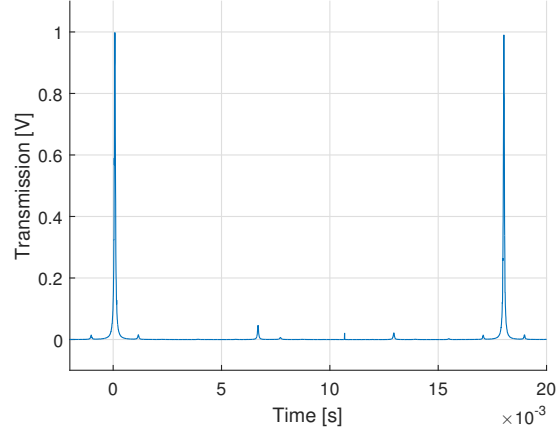
Fig. 7: Single free spectral range of mode cleaner in p-polarization taken by driving the cavity PZT with a $200V_{pp}$ ramp at 10Hz.
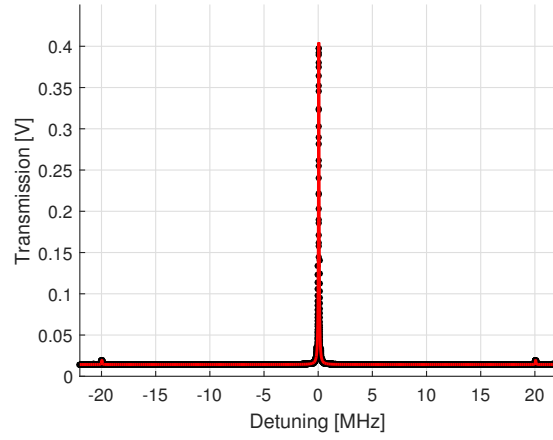

Fig. 8: TEM$_{00}$ transmission through mode cleaner cavity in s-polarization. 20MHz sidebands are used to calibrate detuning. Red trace is a Lorentzian fit to data.

Figure 8 shows how the cavity linewidth is calculated from data. A Lorenzian (with sizebands) is fit to the time-trace voltage of the transmission photodetector, and since the sidebands are known to be at $\pm$20MHz they can be used to transform the x-axis units from time to frequency (assuming that the PZT behaves linearly). The linewidth of the resonance can be extracted from the fit parameters, which for the example above gives $\kappa = 2\pi \times 71.6$kHz.

An optical cavity's finesse F is defined as:

$$F = \frac{\Delta\nu_{FSR}}{\kappa/2\pi} \, ,$$ (6)

which is the number of resonance linewidths that would fit into the FSR. Finesse is purely determined by losses in the cavity and is independent of cavity length.

The mode cleaner cavity has a higher finesse in the s-polarization than the p-polarization due to birefringence effects of the cavity mirror coatings. All measurements described above were taken for both polarizations.

Important parameters of the mode cleaner cavity tested are summarized in Table 1.

Table 1: Mode Cleaner Optical Properties

Polarization	FSR	$\kappa/2\pi$ (FWHM)	F
p	357MHz	1.08MHz	331
s	357MHz	71.6kHz	4990

3.2 Pound-Drever-Hall Locking

In order for the mode cleaners to function properly, they must be locked on resonance. In this experiment the IR mode cleaner will be locked to the main laser using the Pound-Drever-Hall (PDH) technique, a widely used procedure in modern optics experiments. An excellent overview of PDH locking can be found in [Black (2001)].

The PDH technique essentially uses the RF sidebands of a modulated laser as phase references. The sidebands do not interact with the cavity since they are far off resonance, however the carrier will shift in phase. Interfering the sidebands and reflected carrier on a photodetector results in a beat pattern whose phase corresponds to the carrier phase, which uniquely shows whether the laser frequency is below or above cavity resonance.

A traditional layout of the equipment needed for a PDH lock is shown in Figure 9. A laser is sent through a phase modulator driven by a local oscillator to generate sidebands and is then reflected off of a cavity where the carrier and sidebands are collected onto a photodetector. The photodetector signal is mixed with the local oscillator and low-pass filtered to extract the error signal which is then sent to a servo, usually a PID controller, which actuates on the laser to maintain the resonance condition. A phase shifter is needed to ensure that the phases of the two signals going to the mixer are matched.

The PDH lock used for the mode cleaner in the squeezing experiment has several notable differences from the diagram. Rather than feeding back to the laser, the servo is used to control the cavity PZT ensuring that the cavity remains locked to the laser. The other more important distinction is that the electronic signal paths and components are not separate objects. Part of this project focused on implementing an entire PDH lock with a single FPGA using PyRPL. All modulation/demodulation, filtering, and PID control take place within the board.
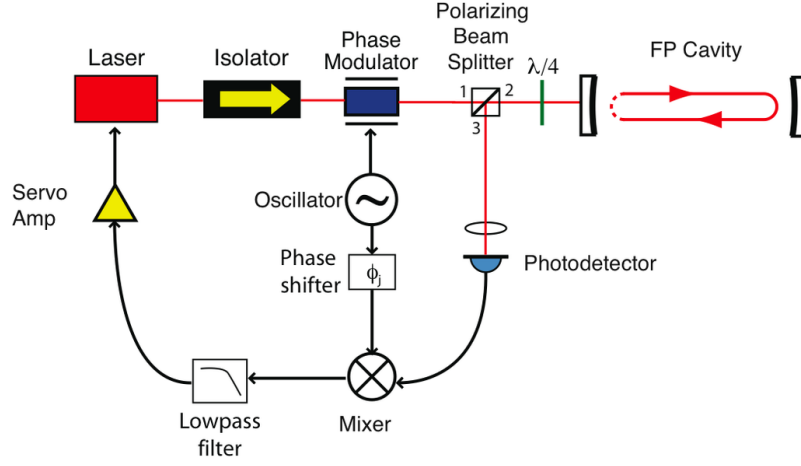
Fig. 9: Pound-Drever-Hall control loop. Red and black traces are optical and electric signal paths respectively. Image credit: Wikipedia

The PDH error signal is generated within the IQ module of PyRPL. A block diagram of the module configured to create this error signal is shown in Figure 10. All necessary modulation/demodulation stages are contained within the module. For the mode cleaner PDH lock specifically, the reflected photodetector signal is sent to the "input_signal" channel, where it is then mixed with an internal local oscillator (with tunable phase offset ϕ). The signal is then demodulated via two low pass filters and scaled according to the "quadrature factor". The "output_signal" (now the PDH error signal) is then sent to a PID controller for feedback. The "output_direct" channel sends the local oscillator signal to the on-table EOM.
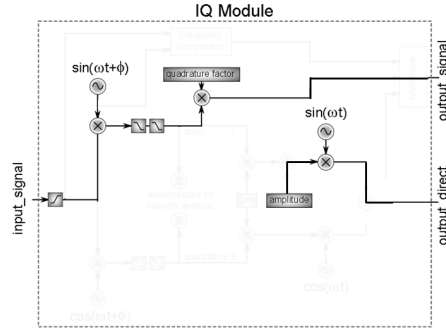

Fig. 10: IQ Module within PyRPL configured for generating PDH error signal.

Figure 11 shows the PDH error signal generated using the IQ module, as well as the corresponding transmission feature. After the correct error signal is generated, the signal is sent to a PID controller. The PID controller attempts to bring the error signal to zero by driving the PZT so that the cavity stays on resonance with the laser. Using the methods described above, the IR mode cleaner was successfully locked to the main

laser. Figure 12 shows a demonstration of the multistage locking described earlier in this report. At time $t = -2.5$s a side-of-fringe lock is engaged, allowing partial transmission of light through the cavity. This lock is held for one second before switching to a PDH lock on resonance at $t = -1.5$s where maximum transmission is achieved.
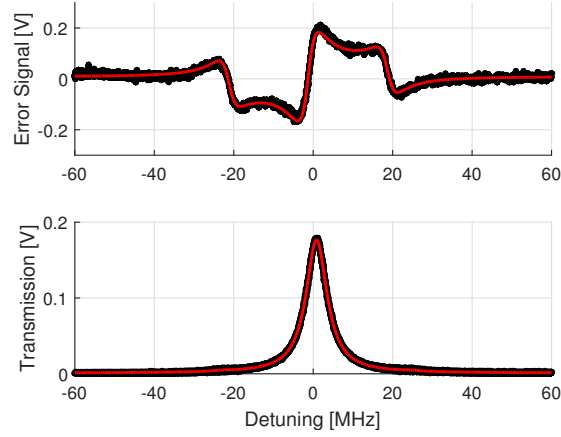

Fig. 11: Red Pitaya generated Pound-Drever-Hall error signal and measured IR mode cleaner cavity transmission. Small sidebands at 20MHz are present. Red traces are fits to data.

3.3 Lock Tuning

Increasing the robustness of the lock requires measuring the transfer function of the closed feedback loop. A basic block diagram of the laser-cavity system and PID controller is shown in Figure 13.

The plant block $P(s)$ is the combined transfer function of the laser, cavity, and photodetector responses. The control block $C(s)$ represents the PID controller, high voltage amplifier, and analog filter low pass filer (used for filtering the noisy high voltage amplifier). The closed loop transfer function $C(s)P(s)$ is measured by injecting a signal $na(s)$ in the loop using the network analyzer function of the FPGA. The network analyzer measures the ratio of the PID output to the injected signal, $pid(s)/na(s)$. It can be shown from the block diagram that

$$pid(s) = C(s)iq(s) \tag{7}$$
$$iq(s) = P(s)out(s) \tag{8}$$
$$out(s) = na(s) + pid(s) \tag{9}$$

where $iq(s)$ is the output of the IQ module (i.e. the error signal) and $out(s)$ is the sum of the PID output and the NA measurement signal. Several lines of straightforward algebra then yield the equation

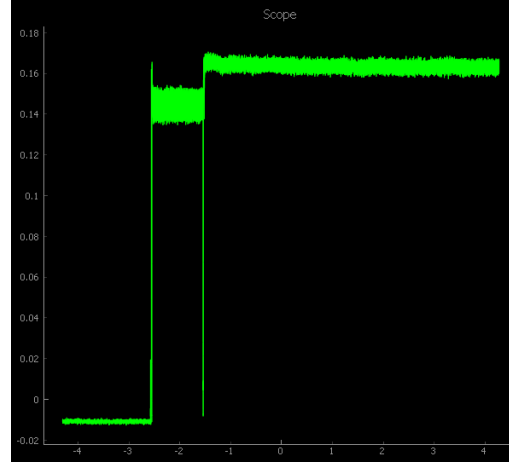$$C(s)P(s) = \frac{\frac{pid(s)}{na(s)}}{1 + \frac{pid(s)}{na(s)}} , \tag{10}$$

Fig. 12: Measured cavity transmission during multistage locking scheme. A side-of-fringe lock is engaged at time $t = -2.5$s, followed by a PDH lock on resonance one second later.
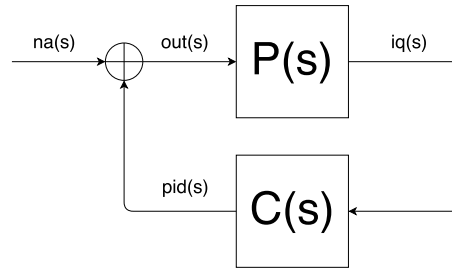

Fig. 13: Closed loop transfer function.

which shows how to reconstruct the closed loop transfer function of interest from the network analyzer data.

Settings in the PyRPL config file allow the user to set the desired unity gain frequency (UGF) of the closed loop transfer funtion. This is implemented by scaling the UGF of the PID module's integrator stage according the the user entered UGF and external filters (e.g. the low-pass filter on the PZT high voltage amplifier).
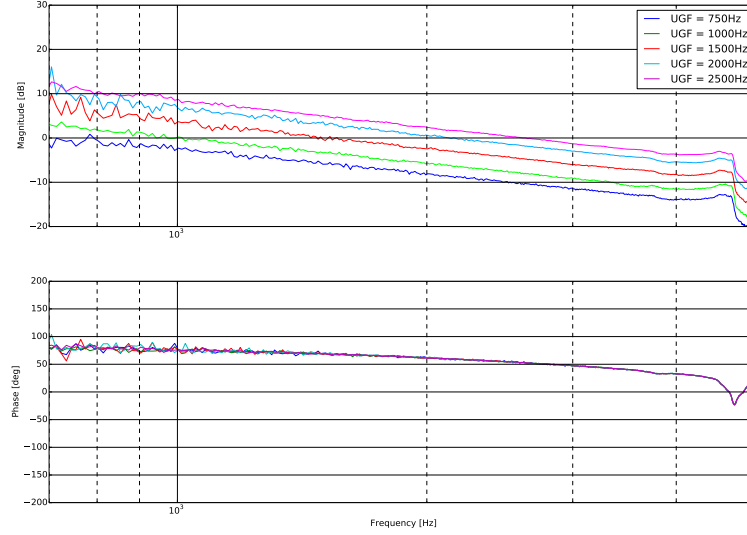
Fig. 14: Closed loop transfer function of the PDH lock. A mechanical resonance occurs around 4.5kHz.

This data was taken using the network analyzer function of PyRPL, which drives the system of interest with a swept sine wave and measures the amplitude and phase response. The transfer functions show an integrator response (1/f falloff, or -20dB/decade) as expected, and the UGF parameter of the PyRPL config file appears to be properly calibrated. A mechanical resonance at around 4.5kHz, potentially from a vibration mode of the IR-MC cavity metal spacer, is the first noise peak that must be attenuated in order to improve lock performance. The first PZT resonance was measured to be around 27kHz.

The lock is fairly robust using these settings; the cavity stays will remain in lock when the optical bench is perturbed, lab doors open/close, etc. However, when the full squeezing experiment is built it will be desirable for the lock to be as stable as possible in order to take long measurements. Improving lock quality can be done through tuning the PID controller, implementing additional filters, and adding extra integrator stages.

4 Rotation Cavity

As its name suggests, the rotation cavity serves to "rotate" the squeezed ellipse (recall Figure 4). The standard quantum limit (SQL) of the system under interrogation deter-

mines where the rotation from amplitude-squeezing to phase-squeezing needs to occur. Since the squeezed light will eventually be used to probe the optomechanical system, the rotation cavity should have a linewidth around 200kHz.

4.1   Optical Characterization

The rotation cavity requires identical measurements as performed on the mode cleaner cavity. Again the cavity PZT is swept to cover a full FSR in order to couple the laser into the TEM_{00} mode, shown in Figure 15.
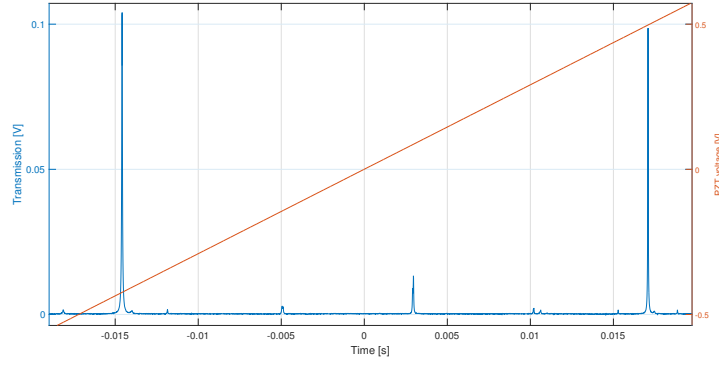

Fig. 15: Single free spectral range of rotation cavity. The PZT is driven by a 10Hz, $200V_{pp}$ ramp.

Two adjacent TEM_{00} modes can be seen around $t = -15$ms and $t = 17$ms. The first even order mode, TEM_{20}, is passed at $t = 3$ms and is caused by mode mismatch. Light in this mode is used as part of a higher order mode locking scheme, discussed later in this report.

The linewidth of the cavity is again measured by fitting a Lorentzian curve with 20MHz sidebands, as in Figure 16. The cavity has a linewidth of $\kappa = 2\pi \times 320$kHz. This is a critical parameter for the squeezing experiment since the half width at half maximum (i.e. $(\kappa/2\pi)/2$) sets the rotation corner where amplitude squeezing and phase squeezing are equal which should correspond to the SQL of the optomechanical system. Optical characteristics of the rotation cavity are summarized in Table 2.

Table 2: Rotation Cavity Optical Properties

Polarization	FSR	$\kappa/2\pi$ (FWHM)	F
P	319MHz	320kHz	997
S	319MHz	330kHz	967

4.2   Spatial Higher Order Mode Locking

Spatial higher order mode locking is a laser locking technique that takes advantage of the TEM_{20} which is a result of the ever-present imperfect mode matching to a cavity. The
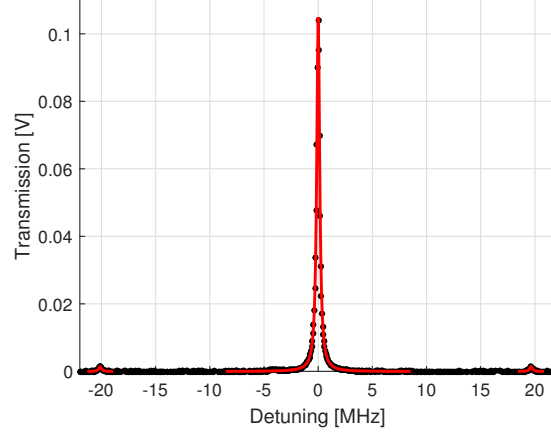
Fig. 16: TEM$_{00}$ transmission through rotation cavity. 20MHz sidebands are used to calibrate detuning. Red trace is a Lorentzian fit to data.

technique was analyzed and demonstrated in [Miller and Evans (2014)] and essentially uses the TEM$_{20}$ mode as a phase reference that doesn't interact with the TEM$_{00}$ cavity mode (rather than using RF sidebands as in PDH locking). The main advantage of this technique is that it doesn't require RF modulation/demodulation of the laser as in PDH locking which often involves costly EOMs.

Generating the higher order mode locking error signal requires either a "bullseye" photodetector, consisting of two concentric detector regions of different radii, or two conventional photodetectors and an iris. The lock implemented on the rotation cavity uses the latter, where the light reflected off the cavity is split into two paths— one path goes straight to a photodetector and the other path is clipped by the iris before reaching a separate photodetector. In either case, the error signal is created by measuring the interference between the two modes whose intensity profiles are shown in Figure 17.
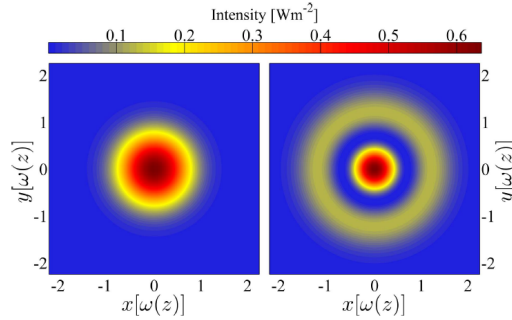

Fig. 17: Intensity profiles of the TEM$_{00}$ and TEM$_{20}$ modes respectively. Image credit: [Miller and Evans (2014)]

Although the modes are orthogonal, the interference term can still be measured by sampling only a portion of the reflected light. The iris serves to clip the outer halo of the TEM_{20} mode, so that the photodiode downstream measures the interference between the central intensity regions of both modes. The additional unclipped photodiode is used to subtract the contribution of the TEM_{00} resonance reflection dip from the error signal.

The error signal generated using this technique is shown in Figure 18. PyRPL makes a theoretical fit to the signal that is the summation of a Lorentzian and derivative of a Lorentzian.
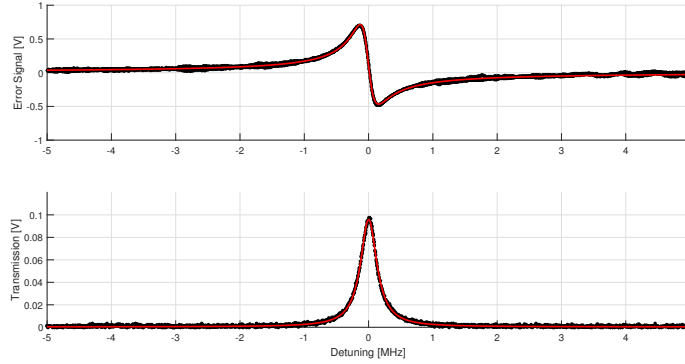

Fig. 18: Higher order mode locking error signal and cavity transmission. Red traces are fits to data.

Once the error signal is generated, PyRPL can lock the rotation cavity to the main laser using the same techniques described above. Higher order mode locking will also be used to eventually look the green mode cleaner cavity.

5   Nonlinear Optics

The ExSqueez-HF experiment will use nonlinear optical processes to produce squeezed light. Nonlinear optics is the field of optics where the polarization response of the medium, with respect to an applied electric field, is nonlinear. The polarization density of a dielectric material P in response to an applied external electric field E can be expanded in a Taylor series as:

$$P = \epsilon_0(\chi_1 E + \chi_2 E^2 + \chi_3 E^3 + ...) \tag{11}$$

where ϵ_0 is the permittivity of free space. Both nonlinear optical elements in the squeezing experiment facilitate a second order interaction, i.e. χ_2 is the dominant coefficient. These χ_2 interactions, also known as three-wave mixing processes, are sum frequency generation and parametric down-conversion.

Sum frequency generation occurs when two low energy photons are converted into a single high energy photon. Parametric down-conversion is essentially the reverse process where one high energy photon is converted into two low energy photons. For the squeezed light experiment, the processes of interest specifically involve the low energy photons being the same energy. These have the specific names of Second Harmonic Generation and Optical Parametric Oscillation. Both processes are illustrated in Figure 19 below.

(a) Second Harmonic Generation.   (b) Optical Parametric Oscillation.

Fig. 19: Two χ_2 nonlinear processes.

Both processes must satisfy the conservation laws of energy and momentum. A photon with angular frequency ω has energy $E = \hbar\omega$. Conservation of energy then gives

$$\sum_{in} \omega_i = \sum_{out} \omega_j \,, \tag{12}$$

where the sums are taken over all incoming and outgoing photons respectively. Photons also carry linear momentum $\boldsymbol{p} = \hbar\boldsymbol{k}$, where $\boldsymbol{k}$ is the wave vector. The equivalent conservation of momentum statement is then

$$\sum_{in} \boldsymbol{k}_i = \sum_{out} \boldsymbol{k}_j \,. \tag{13}$$

Both conservation laws together imply that the refractive index n of the nonlinear medium must be equal for all incoming and outgoing photon frequencies, known as phase matching. However nonlinear media are typically dispersive, meaning that the refractive index has a dependency on frequency $n(\omega)$. Efficient phase matching can still be achieved but requires other methods to counteract dispersion. Birefringent phase matching relies on different polarizations of the input and output fields. Quasi-phase matching involves periodically changing the crystal domain structure which modulates the nonlinear coefficient, known as periodic poling.

6   Second Harmonic Generator

Second harmonic generation is a special case of sum frequency generation where both lower energy photons are the same frequency. In the full squeezing experiment, the second harmonic generator (SHG) will be used to convert the main laser at 1064nm into a frequency doubled beam at 532nm. The SHG consists of a magnesium-oxide-doped lithium niobate (MgO:LiNbO$_3$) crystal inside of a Fabry-Perot cavity, where the crystal provides the nonlinear interaction and the cavity effectively increases the nonlinear gain by causing the main laser light to pass through the crystal many times. Lithium niobate relies on birefringence to achieve phase matching, specifically Type I where the main field is polarized along the material ordinary axis and the harmonic field is orthogonally polarized along the extraordinary axis.

Achieving a high conversion efficiency from IR to green photons requires both a robust cavity lock to the main laser and a stable crystal temperature that facilitates optimal phase matching. Once the SHG was assembled and aligned, the cavity was PDH locked in transmission using PyRPL as described above. Once the cavity is locked, the crystal temperature can be scanned using a standard TEC controller which drives a peltier attached to the crystal. These two processes are nontrivial since they are coupled together— when the cavity is locked laser power builds up and increases the temperature,

but increasing the temperature also leads to thermal expansion of the cavity which the PDH lock tries to fight by compensating with the PZT.

Ultimately the optimal working temperature for the SHG was found to be at 85°C. When locked at this temperature, around 120mW of green light is produced. The full squeezing experiment requires an estimated 100mW of green in order to compensate for optical losses downstream. Figure 20 shows green light being produced from the SHG.
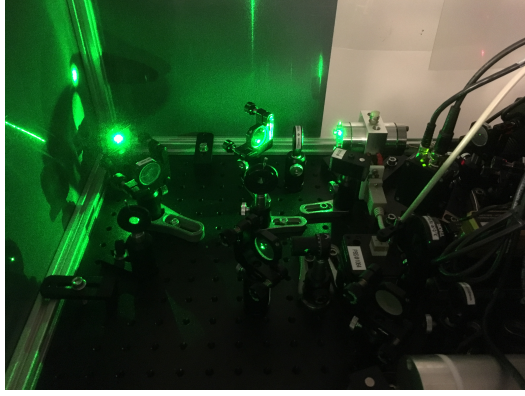

Fig. 20: SHG (on the far right) converting IR light into green light.

7   Optical Parametric Oscillator

A degenerate optical parametric oscillator (OPO) will be used in the squeezing experiment to convert pairs of green photons at 532nm (generated with the SHG) back into IR photons at 1064nm. A small "seed" beam of IR light is sent into the OPO, which then stimulates the green "pump" photons to decay into IR photons, which amplifies the seed. This amplified seed beam has correlated sidebands pairs as a result of this process; these correlated sidebands result in bright frequency independent squeezed light.

The OPO consists of a nonlinear crystal inside of a bow-tie cavity that is doubly resonant to both 1064nm and 532nm light, as in Figure 21. The crystal material is periodically-poled potassium titanyl phosphate (PPKTP), so it relies on Type 0 quasi-phase matching.

7.1   Phase matching

The OPO employs a similar temperature control system as the SHG to achieve phase matching. Rather than measuring the temperature directly, the TEC controller measures and feeds back on the resistance of a thermistor. The conversion from thermistor resistance to temperature was found by fitting the Steinhart-Hart equation to data provided in the spec sheet. The optimal temperature for phase matching was experimentally determined by injecting the OPO with IR light from the main laser to generate green light (the crystal can be used for both second harmonic generation and optical parametric oscillation). A photodiode was used to record the power of green light generated while the TEC controller swept through a range of temperatures, as shown in Figure 22.
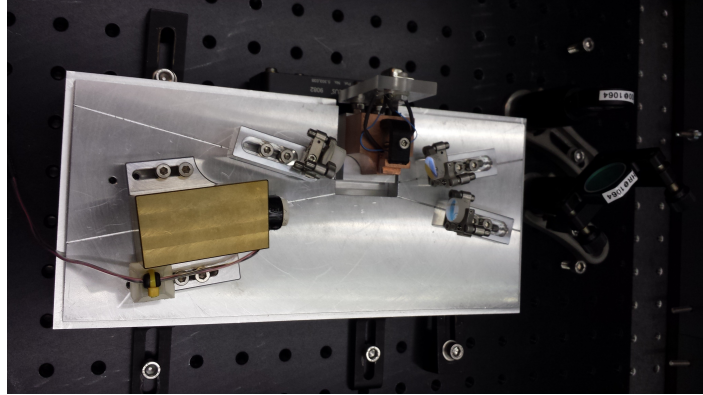
Fig. 21: Optical parametric oscillator, containing a temperature controlled PPKTP crystal inside of a bow-tie cavity.
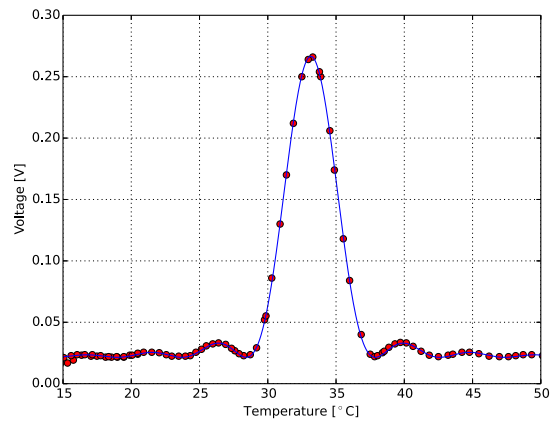

Fig. 22: Nonlinear gain of OPO as a function of temperature. Blue trace is a sinc^2 fit.

The data was fit to a squared sinc function as theoretically predicted [Boyd (1992)]. The optimal crystal temperature was determined to be 33.15°C, which will be used as the set point in the full squeezing experiment. The offset of 21.5mV is a result of residual IR light leaking through the OPO and dichroic mirrors onto the photodetector.

8   Future Work

ExSqueez-HF will require several more weeks of work before frequency dependent squeezed light is generated and measured. The SHG will need to produce more green light which requires an increase in conversion efficiency or a more power in the injected IR light. Now that a source of green light is available, the green mode cleaner will need to be characterized and locked using the same higher order mode locking as the rotation cavity. An additional PDH lock will also need to be implemented for the OPO bow-tie cavity.

Measuring both frequency dependent and frequency independent squeezing will require building a homodyne detection stage. The ultimate goal of the experiment is to inject frequency dependent squeezed light into the micropillar system in order to demonstrate sub-SQL quantum noise reduction. This will require moving the ExSqueez-HF experiment to a different optical table and interfacing with the micropillar experiment.

Rather than using the bright, high frequency squeezing that will be generated with the ExSqueez-HF experiment, gravitational wave detectors will inject a low frequency squeezed vacuum state into the dark port of the interferometer in order to reduce quantum noise. Generating this type of squeezing is considerably more difficult for several technical reasons. Since squeezed vacuum has no coherent amplitude, more precautions must be made to prevent stray light from entering into the homodyne detection stage. It is also typically necessary to place the entire homodyne detection stage in a vacuum chamber in order to reduce air currents and noise due to gas particles buffeting optical elements. A low rotation frequency will require a much more narrow linewidth rotation cavity, on the order of 100Hz. Such cavities are an area of active research at LAL (Laboratoire de l'Accelerateur Lineaire) in Orsay, specifically on their test facility called CALVA. The Optomechanics and Quantum Measurements group is finalizing the design of a low frequency squeezed light source that will interface with CALVA, known as the ExSqueez-LF experiment.

Acknowledgements

Bibliography

Black, E. D. (2001). An introduction to pound–drever–hall laser frequency stabilization. *American Journal of Physics*, 69(1).

Boyd, R. W. (1992). *Nonlinear Optics*. Academic Press.

Caves, C. M. (1981). Quantum-mechanical noise in an interferometer. *Phys. Rev. D*, 23:1693–1708.

Chua, S. S. Y., Slagmolen, B. J. J., Shaddock, D. A., and McClelland, D. E. (2014). Quantum squeezed light in gravitational-wave detectors. *Classical and Quantum Gravity*, 31(18):183001.

Kuhn, A. G., Teissier, J., Neuhaus, L., Zerkani, S., van Brackel, E., Deléglise, S., Briant, T., Cohadon, P.-F., Heidmann, A., Michel, C., Pinard, L., Dolique, V., Flaminio, R., Taïbi, R., Chartier, C., and Le Traon, O. (2014). Free-space cavity optomechanics in a cryogenic environment. *Applied Physics Letters*, 104(4).

LSC (2016). Observation of gravitational waves from a binary black hole merger. *Phys. Rev. Lett.*, 116:061102.

Miller, J. and Evans, M. (2014). Length control of an optical resonator using second-order transverse modes. *Opt. Lett.*, 39(8):2495–2498.